Jaroslav Vaculik, Michael C. Griffith
Out-of-plane load-displacement model for two-way spanning masonry walls
Engineering Structures, 2017; 141:328-343

Final publication at http://dx.doi.org/10.1016/j.engstruct.2017.03.024

This is a pre-copyedited, author-produced version of an article accepted for publication in *Engineering Structures* following peer review. Publisher's version is available online at the following link:
doi: 10.1016/j.engstruct.2017.03.024
(Citation information found therein)

Out-of-Plane Load-Displacement Model for Two-Way Spanning Masonry Walls

Jaroslav Vaculik[a,*], Michael C. Griffith[a]

[a] *School of Civil, Environmental and Mining Engineering, The University of Adelaide, SA 5005, Australia*

Abstract

This paper describes a methodology for modelling the nonlinear, inelastic load-displacement behaviour of two-way spanning unreinforced masonry walls subjected to out-of-plane loading. The model utilises a simplified macroblock approach that starts with the assumption of a collapse mechanism based on the wall's boundary conditions. It then treats the wall as having zero tensile strength and assumes that the resistance comes entirety from two gravity-based resistance components: elastic rigid block rocking, and inelastic friction, with the total load resistance of the wall taken as the sum of these individual components. Analytical expressions for calculating the load and displacement capacities of the elastic rocking component of response are derived from the principles of statics using an integration approach well suited for the treatment of two-way mechanisms. Expressions for the associated frictional capacity component are obtained using the virtual work method. Comparison of the theoretical load-displacement response with experimentally measured data is favourable as demonstrated using data obtained via quasistatic cyclic tests on two-way spanning walls; the model is shown to provide an acceptable lower bound estimate of actual behaviour. The developed approach could be used to construct pushover curves for a range of different collapse mechanisms and therefore has the potential to be assimilated into a simplified displacement-based seismic design/assessment technique for two-way spanning walls against out-of-plane collapse.

Keywords: Unreinforced masonry, load-displacement capacity, hysteresis model, displacement-based seismic assessment

1. Introduction

Despite the common perception that unreinforced masonry (URM) structures are brittle, the collapse of URM walls subjected to out-of-plane earthquake loading is governed by geometric stability rather than tensile strength, and the associated load-displacement (F-Δ) behaviour can be considered pseudo-ductile. This can be explained by the fact that the formation of cracks and attainment of ultimate load capacity occur early in the overall out-of-plane F-Δ response (illustrated in Figure 1), which is followed by a reduction in load resistance as a collapse mechanism develops. Once fully cracked, the wall undergoes rocking type behaviour before it eventually becomes destabilised by gravity.

This behaviour is already well established for one-way vertically spanning URM walls (either free standing or simply-supported at top and bottom) whose F-Δ response is nonlinear but elastic, and whose idealised displacement (instability) capacity is equal to the wall thickness [1–4]. By contrast, cyclic loading tests on *two-way spanning* brick walls (walls supported by a combination of their vertical and horizontal edges) have demonstrated that their displacement capacity can be even larger than the wall thickness [5]. This is due to two main reasons: vertically rotating subpanels present in two-way wall mechanisms are not destabilised by gravity, and vertical cracks with brick interlock exhibit bed joint friction which is inherently ductile. The aforementioned cyclic tests as well as shaketable tests on similar half-scale walls [6] have also shown two-way walls to exhibit moderate hysteretic damping due to frictional sources of resistance, which is further beneficial to their seismic performance.

Conventional force-based (FB) seismic design, where the objective is to ensure that the wall's load capacity exceeds the imposed load demand, continues to be the most commonly used method for designing URM walls against out-of-plane failure. From the designer's point of view, this approach is most likely to lead to a favourable outcome (in terms of being able to demonstrate a wall's seismic adequacy) if the ultimate load capacity inclusive of bond strength contribution is known. However, in practical assessment of existing URM buildings it is often difficult to reliably quantify the bond strength without extensive destructive testing. And whilst collapse load capacities can be computed using simplified limit analysis techniques that ignore bond strength and instead rely on geometric properties for input (e.g. [7, 8]), these capacities can often be too low to demonstrate adequacy despite the wall having additional displacement capacity which may save it from collapse under earthquake excitation. Therefore, it is of considerable practical interest to develop an alternate tool for out-of-plane URM

*Corresponding author
Email addresses: jaroslav.vaculik@adelaide.edu.au (Jaroslav Vaculik), michael.griffith@adelaide.edu.au (Michael C. Griffith)

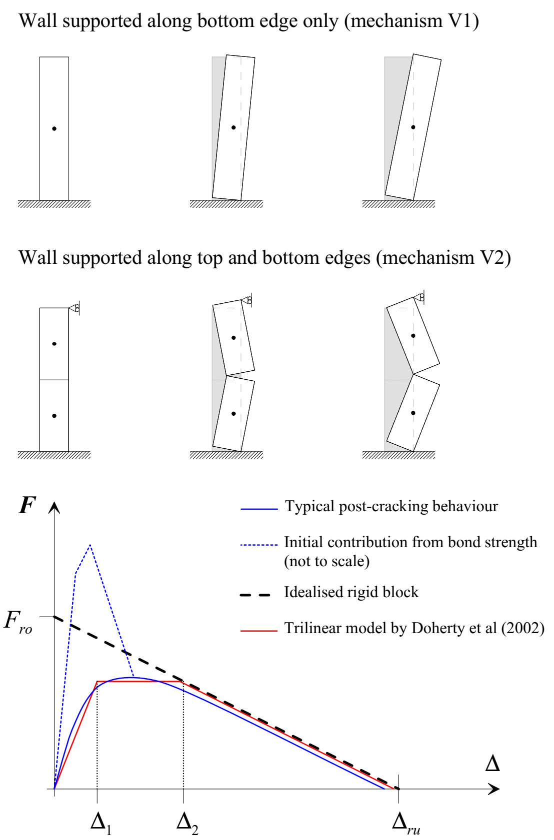

Figure 1: Rocking behaviour of vertically spanning walls. (Only positive displacement side is shown)

wall design/assessment that does not rely on knowledge of the bond strength and which allows for this reserve capacity to be utilised.

Recent trends in seismic design of ductile structural systems have seen a move away from force-based (FB) techniques and toward displacement-based (DB) methods [9], where the design objective is to ensure that the displacement capacity exceeds the displacement demand. Amongst the appeal of DB philosophy is that by accounting for the full displacement capacity, it avoids some of the aforementioned over-conservatism inherent in the FB approach. The fundamental feature of the DB method is that it estimates the structural period using a secant stiffness at the target level of displacement response (instead of using the initial elastic stiffness with subsequent application of load reduction factors to account for ductility effects as is done in FB design). This framework can be implemented in various forms such as direct DB design [10] or the capacity spectrum approach [11]; however, each relies on the ability to construct a F-Δ capacity curve for the structure (in this case the wall).

Considerable progress has already been made toward development of DB methodology for vertically spanning URM walls subjected to rocking. The associated F-Δ capacity rules can be broadly categorised into two types, as illustrated in Figure 1. The first is based on idealised rigid block treatment characterised by linear-descending branches in the positive and negative Δ domains with a discontinuity at $\Delta = 0$. The dynamics of such a system were originally described by Housner [12] and first applied to masonry walls by Priestley et al [13] and further developed since by others [14–16]. The second type of treatment incorporates an initial linear elastic branch to account for non-rigid behaviour, for example using bilinear or trilinear rules [2, 17–19].

Extension of DB methodology to two-way spanning walls has lagged behind, largely due to the lack of a suitable and experimentally validated model to describe the load-displacement behaviour. Promising progress has however been made on this topic recently by Lagomarsino [19], who developed a generalised procedure for constructing pushover curves for multiple-block rocking mechanisms. The present paper aims to provide further contribution by proposing a technique for constructing pushover curves for a common class of two-way wall collapse mechanisms, which accounts for the nonlinear, inelastic nature of the response, and which can subsequently be used as the basis for a DB methodology for this class of walls.

2. Wall Configurations

Before the analytical F-Δ relationship formulation is described in Section 3, the present section will overview the wall configurations that can be catered for.

2.1. Support Conditions and Collapse Mechanisms

The proposed model starts with the user postulating a collapse mechanism based on the wall's geometry and boundary conditions. Figure 2 illustrates the particular out-of-plane collapse mechanisms which are considered in this paper. This family of mechanisms (referred to here as type K) is characterised by diagonal cracks that radiate from corners at which supported edges intersect, and is the most common class of mechanisms associated with mortar-bonded two-way spanning walls as evidenced through a multitude of experimental studies (e.g. [5, 6, 20–23]). These mechanisms are also embodied in different variations of the plastic analysis method for predicting the ultimate strength of two-way URM walls, including methods prescribed by the Australian Standard and Eurocode 6 [24, 25].

The boundary conditions necessary to generate these mechanisms include translational support at the bottom edge and at least one vertical edge. The top edge can be either free (type K1 mechanisms) or restrained (type K2 mechanisms). For conciseness, Figure 2 shows the wall to be supported along both of its vertical edges; however, each mechanism can also have a form where only a single vertical edge is supported, which is equivalent to considering only one half of the shown deflected shape on either side of the vertical line of symmetry.

It should be mentioned that a wall with a particular set of boundary conditions can potentially undergo additional types of collapse mechanisms to those considered here [7, 8], and that since the method adopted is a form of upper bound limit analysis, in a design situation it may be necessary to check a wall against several alternate possible forms to identify the critical one. A study comparing collapse loads computed using

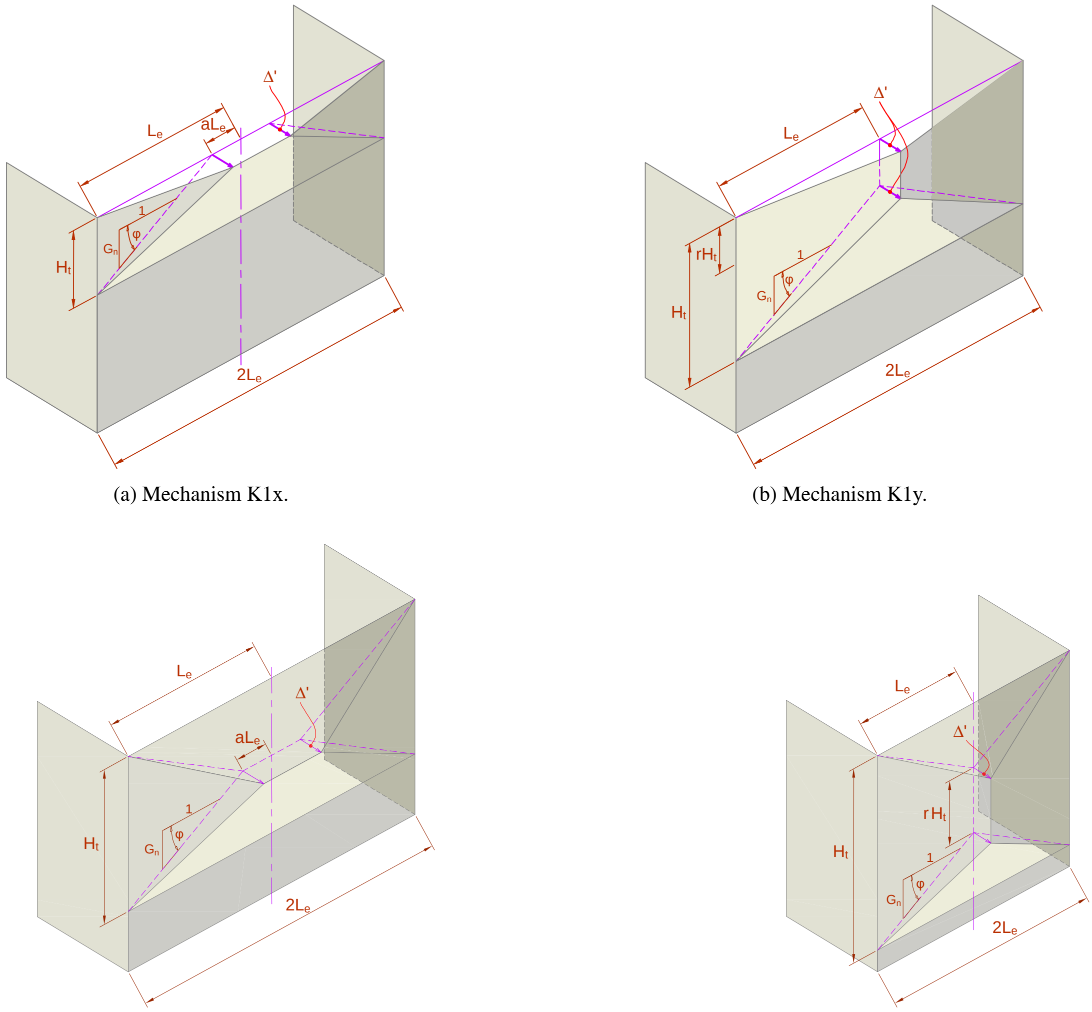

(a) Mechanism K1x.

(b) Mechanism K1y.

(c) Mechanism K2x.

(d) Mechanism K2y.

Figure 2: Type K mechanisms. The location of the reference displacement in each mechanism is indicated as Δ'.

different types of two-way mechanisms in walls free at the top edge has shown that mechanism K1 tends to be kinematically favoured in walls with relatively strong bond prior to crack formation [26]. By contrast, walls with zero or low bond strength are more likely to develop mechanisms characterised by diagonal cracks propagating inwards in a 'V' shape (such as mechanisms type D and G dealt with in [7, 8]). Although this paper deals solely with type K mechanisms, the general procedure described can similarly be applied to other forms. It should also be noted that the total height of a two-way mechanism may not necessarily be equal to the full height of the wall as illustrated in Figure 2; however, this will not be discussed further here as it is dealt with in other works [8, 26].

In the equations featured in this paper, the following notation will be used: H_t and L_t are the total height and length of the mechanism, respectively; G_n is the slope of the diagonal crack. In the case of half-overlap stretcher bond masonry (Figure 3), this slope follows one bed joint across, one perpend joint up (and so on), and is given by:

$$G_n = \frac{2\left(h_u + t_j\right)}{l_u + t_j}, \tag{1}$$

where l_u, h_u and t_u are the length, height and thickness of the masonry unit, and t_j is the mortar joint thickness.

The effective height and effective length of the mechanism are taken as

$$H_e = H_t/n_{hs}, \tag{2}$$

$$L_e = L_t/n_{vs}, \tag{3}$$

where n_{hs} and n_{vs} are the number of supported horizontal and vertical edges, respectively. From these definitions, the effective aspect ratio of the mechanism is defined as

$$\alpha = G_n \frac{L_e}{H_e}. \tag{4}$$

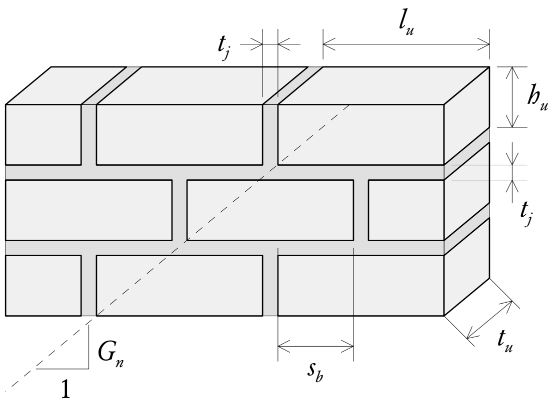

Figure 3: Basic notation for half-overlap stretcher bond masonry.

Referring to Figure 2, it is seen that $\alpha = 1$ is the limiting case between the complimentary x and y pairs of the K1 and K2 mechanisms. With this in mind, we define the additional shape parameters:

$$a = 1 - 1/\alpha \qquad \text{for } \alpha \geq 1, \tag{5}$$

and

$$r = 1 - \alpha \qquad \text{for } \alpha \leq 1. \tag{6}$$

In the context of practical DB seismic assessment it is important to note that ignoring the presence of a top edge support and assuming that a wall undergoes mechanism K1 instead of K2 may not necessarily be conservative, because whilst K2 will generally have a higher load capacity, K1 will have a higher displacement capacity (instability displacement). The reason for this is that mechanism K1 exhibits a greater degree of rotation about the vertical axis and so its subpanels become less destabilised by gravity. This argument is supported by experimentally observed behaviour [5] and can also be demonstrated using analytical equations presented later in the paper (refer Table 1). Where both mechanisms are possible (case of a frictional top connection), a seismic assessment should consider both and adopt the critical one.

For comparison purposes, this paper will also consider one-way vertically spanning versions of these mechanisms in which both vertical edges are unsupported; these will be referred to as V1 where only the bottom edge is laterally restrained, and V2 where both the top and bottom edges are restrained, as illustrated in Figure 1.

2.2. Loadbearing Walls

Allowance is made for the presence of a precompression load at the top of the wall due to for example a floor system or another part of the building's mass. If we define σ_{vo} as the applied precompression stress at the top edge, then a convenient way to represent the imposed load is in the nondimensional form:

$$\psi = \frac{\sigma_{vo}}{\gamma H_t}, \tag{7}$$

where γ is the weight density of the masonry, and ψ can be interpreted as the ratio of the overburden weight to the weight of the wall involved in the collapse mechanism. Presence of the precompression load acts to enhance a wall's load resistance by increasing the internal moment capacities along the various crack lines in the mechanism; however, it can also give rise to additional effects which will now be discussed.

2.2.1. Restraint of the Precompression Load

In mechanisms where the top edge of the wall is free (K1 and V1) it is important to consider whether the mass imposing the precompression is restrained from horizontal movement (e.g. stiff slab tied to in-plane walls), or unrestrained (e.g. flexible diaphragm floor).

This effect is demonstrated in Figure 4, where it is seen that each scenario imposes a lateral load on the top edge. If the mass is restrained but not positively connected to the wall (Figure 4a), then frictional slip at the top interface generates a restoring force $\mu_o\psi$, where μ_o is the friction coefficient at the interface. By contrast, if the mass is unrestrained (Figure 4b), then under inertial loading it will apply an additional destabilising force $\lambda\eta\psi$, where λ is the lateral load multiplier (acceleration in units of g's) and η is the ratio of the precompression weight free to act laterally to its vertical action on the wall. The factor η is introduced simply because the horizontally and vertically acting components may not necessarily be equal, and in most circumstances its value can be determined directly from statics.

To activate or deactivate these effects in the presented formulation, we introduce the binomial variable Φ, taken as

$$\Phi = \begin{cases} 0 & \text{for a restrained precompression load,} \\ 1 & \text{for an unrestrained precompression load.} \end{cases} \tag{8}$$

2.2.2. Precompression Load Eccentricity

The vertical line of action of the precompression load affects the moment imposed on the wall, which in turn influences the wall's load and displacement capacities. In the developed formulation the precompression eccentricity is specified using the nondimensional parameter ϵ, defined such that the precompression is applied at a distance $\epsilon\, t$ measured from the upward-deflecting point along the top edge. This reference point is located on the windward side in mechanisms where the top edge is unsupported (K1, V1) and on the leeward side when the top edge is restrained (K2, V2), as illustrated in Figure 5.

Because the upward-deflecting point switches sides with alternating Δ direction, it is important to consider the influence of the top edge connection on ϵ under Δ reversal as it can potentially lead to asymmetric F-Δ response. In the case of a point-bearing connection (Figure 5) in which the location of the load transfer point remains fixed relative to the wall, alternating Δ direction causes eccentricity to switch between ϵ^+ and ϵ^-, and thus behaviour will be asymmetric (An exception is when the bearing is positioned at the mid-thickness; $\epsilon = 1/2$). Alternatively, if the precompression load is due to a rotationally stiff element such as a slab whose surface remains horizontal, then the load transfer point will shift with alternating Δ direction such that the load always acts at the upward-deflecting point;

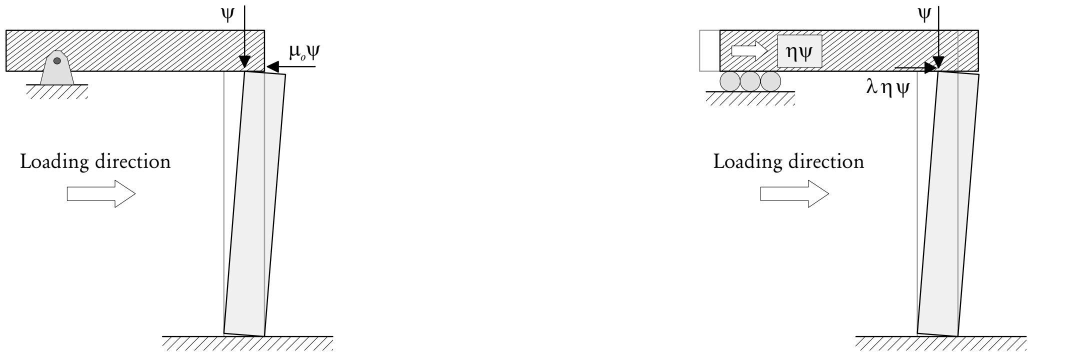

(a) Precompression load restrained ($\Phi = 0$); frictional connection at the top interface.

(b) Precompression load unrestrained against lateral movement ($\Phi = 1$).

Figure 4: Additional loads imposed on a wall by either a restrained or unrestrained precompression load in mechanisms where the top edge is free.

(a) Top edge unsupported.

(b) Top edge supported.

Figure 5: Precompression load eccentricity under reversed displacement direction. The upward-deflecting point relative to which the eccentricity is measured in the proposed formulation is shown by black triangle.

thus $\epsilon = 0$ and response will be symmetric. It can further be demonstrated that the wall receives the maximum benefit toward both its strength and displacement capacities when the load acts at the upward-deflecting point as this generates the maximum possible restoring moment on the wall.

3. Load-Displacement Formulation

For a given collapse mechanism, the theoretical F-Δ relationship is constructed using a nonlinear static analysis that takes the total load resistance (λ) as the superposition of three contributing sources:

$$\lambda(\delta) = \lambda_r(\delta) + \lambda_h(\delta) + \lambda_s(\delta)\,, \tag{9}$$

where λ_r is elastic rigid body rocking (Figure 6a), λ_h is horizontal bending friction (Figure 6b), and λ_s is frictional sliding between the wall and a precompression load (if applicable). Each of these will now be described in greater detail.

For convenience, this paper treats load in the nondimensional form λ, defined as the force divided by the wall's weight, which is equivalent to acceleration in units of g. Displacement is also treated in a normalised form δ, defined as

$$\delta = \Delta/t, \tag{10}$$

where Δ is the actual displacement, and t is the wall thickness.

3.1. General Assumptions

The proposed theoretical approach makes the following general assumptions:

1. The tensile strength of the wall is ignored and the wall is assumed to be already cracked.

2. The wall's displacement profile is assumed to follow an idealised collapse mechanism comprising a series of rigid, flat subpanels bordered by rotating hinge lines (Figure 2). This further assumes that: (a) frictional sliding between subpanels is avoided, and (b) vertical edges remain sufficiently supported against translation following cracking.

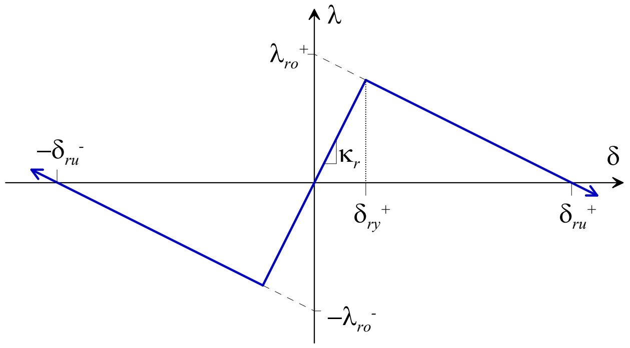

(a) Rocking component $\lambda_r(\delta)$, modelled using elastic bilinear-softening rule.

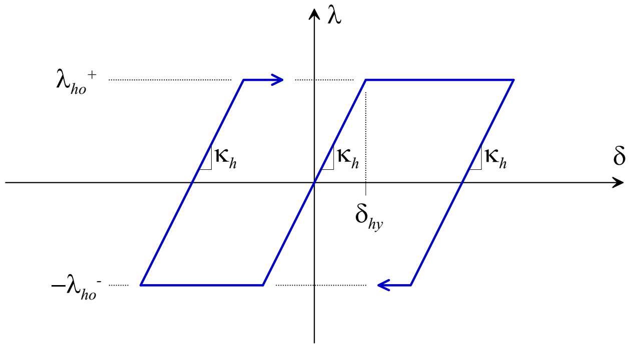

(b) Inelastic component due to horizontal bending friction, $\lambda_h(\delta)$, modelled using elastoplastic rule.

Figure 6: Hysteresis rules for representing various components of the wall's load resistance.

3. The user must make a reasonable approximation of the diagonal crack slope (G_n) which feeds into equation (4). In stretcher bond brickwork, diagonal cracks can be generally assumed to follow the slope G_n as shown in Figure 3; however alternate bond patterns may require different approximations.

4. The lateral load acting on the wall is assumed to be spatially distributed proportionally to the wall's mass; i.e., uniform acceleration λ.

5. Each of the contributing resistance sources (λ_r, λ_h and λ_s) are assumed to be independent so that their contributions can be superimposed as per equation (9).

6. Contributions from internal confinement and arching are ignored. This assumption is conservative as it neglects the the additional load resistance provided by these effects at small displacements. Whilst arching can also provide a destabilising influence at large displacements, this occurs beyond the rigid body instability displacement.

3.2. *Rocking Component*

Rocking response provides the primary component in the overall F-Δ formulation which gives rise to the linear-descending shape of the response and dictates the ultimate displacement capacity (Figure 6a).

To formulate the load-displacement for the rocking component, the two-way mechanism is discretised into a series of vertically spanning strips which are held together by out-of-plane compatibility (Figure 7a). For a generic strip, equations of force and moment equilibrium are formulated under a known reference displacement δ and an unknown load λ. Then, by integrating the moment contribution from each strip along the length and ensuring that moment equilibrium is satisfied, we can obtain an expression that relates λ to δ for the overall mechanism.

The process makes the following assumptions (additional to those in Section 3.1):

1. The vertical strips transmit zero vertical shear force and zero net horizontal shear force across their lateral boundaries (V_{xy} and V_{xz} in Figure 7b).

2. The vertical strips can however transmit moment about the longitudinal axis (x) across these boundaries (M_1, M_2 and M_3 in Figure 7b).

3. Additionally, the initial derivation of the λ-δ relationships (Section 3.2.1) assumes that vertical load transfer across subpanels is concentrated at the extreme edges, which treats the panels as rigid and having unlimited compressive strength. These idealisations are subsequently relaxed in Section 3.2.2 with regard to treatment of real walls.

From the first two assumptions it follows that the entirety of the lateral load is resisted by reactions along the top and bottom edges where supports are provided, shown as R_{1x} and R_{2x} in Figure 7c. Consequently, the vertical edge support receives zero net force reaction (a conservative assumption); however, it does receive a moment reaction about the longitudinal axis, shown as M_{3x} in Figure 7c. As face-loaded two-way spanning walls are statically indeterminate, these assumptions achieve the task of reducing the degree of indeterminacy and allowing statics to be used to solve for the λ-δ relationship.

3.2.1. *Idealised Rigid Rocking Behaviour*

For the purpose of demonstrating the process used to formulate the rigid rocking λ-δ relationship, we shall arbitrarily select mechanism K2x. Let us subject the mechanism to a central (mid-height) displacement Δ_c and consider a generic vertical strip of width $\mathrm{d}x$ as shown in Figure 7a. The geometry of the cross section (Figure 8) is dependent on the shape parameter ρ, which varies along x and assumes values in the range 0 to 1 (Figure 7d). When the section intersects the diagonal cracks ($\rho < 1$) it comprises three blocks.

Since the mechanism has top edge support, from equation (2) we get

$$H_e = \tfrac{1}{2} H_t \quad \text{(for mechanism K2).} \tag{11}$$

Similarly, we define the effective weight as

$$\mathrm{d}W_e = \mathrm{d}x\, t\, H_e\, \gamma. \tag{12}$$

Referring to Figures 7a, 7d and 8, the heights and weights of the respective blocks are:

$$h_\mathrm{v} = \rho H_e, \qquad \mathrm{d}W_\mathrm{v} = \rho\, \mathrm{d}W_e, \tag{13}$$

$$h_\mathrm{h} = (1-\rho)\, H_e, \qquad \mathrm{d}W_\mathrm{h} = (1-\rho)\, \mathrm{d}W_e. \tag{14}$$

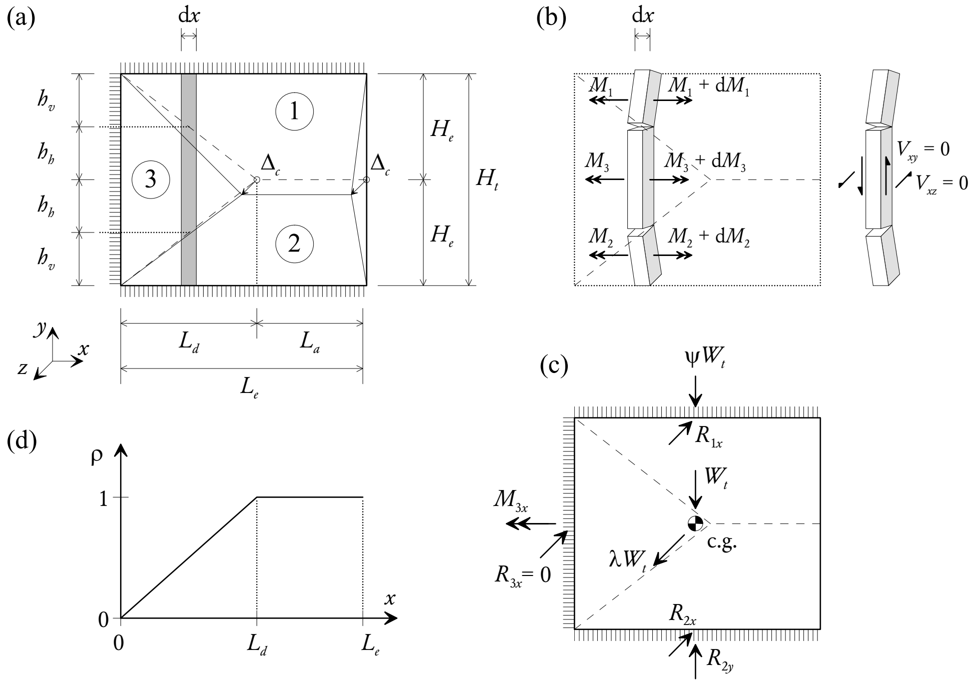

Figure 7: Panel subjected to mechanism K2x; (a) geometry of overall panel and a generic vertical strip; (b) moments and forces acting across boundaries between adjacent strips; (c) external forces acting on the overall panel, including reactions acting on the supported edges as implicit in the proposed method; (d) variation of geometric parameter ρ along the length.

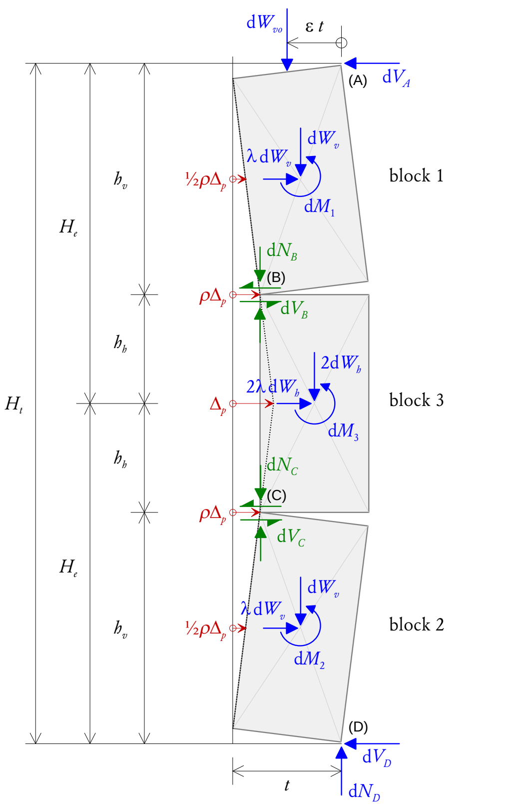

Figure 8: Generic cross section for mechanisms K2x and K2y.

Also noting equation (7), the weight of the precompression load is

$$\mathrm{d}W_{vo} = 2\psi\, \mathrm{d}W_e \quad \text{(for mechanism K2).} \tag{15}$$

As shown in Figure 8, it is convenient to measure the displacement profile along the height of the cross section with respect to a projected mid-height displacement Δ_p, which is related to the maximum mechanism displacement Δ_c (indicated by Δ' in Figure 2) as

$$\Delta_c = \begin{cases} \Delta_p & \text{in mechanisms K1x and K2x,} \\ (1-r)\,\Delta_p & \text{in mechanisms K1y and K2y,} \end{cases} \tag{16}$$

where r is given by equation (6).

The external and internal loads acting on the blocks are shown in Figure 8. There are a total of 10 unknowns: horizontal reactions dV_A and dV_D; internal shear forces dV_B and dV_C; internal axial forces dN_B and dN_C; vertical base reaction dN_D; as well as the moments dM_1, dM_3 and dM_2 acting on the top, middle and bottom blocks respectively. Note that the dN and dV terms are internal forces within each strip. By contrast, the dM terms are increments of moment that each block contributes to the subpanel within which it is situated (refer Figure 7b), and in this sense they can be considered as external actions with respect to each block. Alternatively, dM_3 may be interpreted as the moment that must be applied to the central block in Figure 8 to maintain the block assembly in static equilibrium at the imposed displacement. Of the unknowns, the vertical forces (dN_B, dN_C and dN_D) are readily determined from the three vertical force equilibrium equations (one for each block). This leaves us with seven remaining unknowns and six equations to solve for them: horizontal force equilibrium and moment equilibrium for each block.

Implementing these equilibrium conditions and substituting in equations (13)-(14), we get the following set of equations (expressed using matrix notation for conciseness):

$$\mathbf{A}\mathbf{x} = \mathbf{b} \tag{17}$$

where

$$\mathbf{A} = \begin{bmatrix} 1 & -1 & 0 & 0 & 0 & 0 & 0 \\ 0 & 1 & -1 & 0 & 0 & 0 & 0 \\ 0 & 0 & 1 & 1 & 0 & 0 & 0 \\ 0 & H_e\rho & 0 & 0 & 0 & 1 & 0 \\ 0 & 2H_e(1-\rho) & 0 & 0 & 1 & 0 & 0 \\ 0 & 0 & H_e\rho & 0 & 0 & 0 & 1 \end{bmatrix} \tag{18}$$

$$\mathbf{x}^T = \left\{ \mathrm{d}V_A \quad \mathrm{d}V_B \quad \mathrm{d}V_C \quad \mathrm{d}V_D \quad \mathrm{d}M_3 \quad \mathrm{d}M_1 \quad \mathrm{d}M_2 \right\} \tag{19}$$

$$\mathbf{b}^T = \left\{ b_1 \quad b_2 \quad b_3 \quad b_4 \quad b_5 \quad b_6 \right\} \tag{20}$$

$$b_1 = \rho\lambda\,\mathrm{d}W_e \tag{21}$$

$$b_2 = 2\lambda(1-\rho)\,\mathrm{d}W_e \tag{22}$$

$$b_3 = \rho\lambda\,\mathrm{d}W_e \tag{23}$$

$$b_4 = \left[\left(\tfrac{1}{2}\rho + 2\psi\right)\left(t - \Delta_p\rho\right) - 2\epsilon\psi t - \tfrac{1}{2}H_e\rho^2\lambda\right]\mathrm{d}W_e \tag{24}$$

$$b_5 = \left[2H_e\lambda(1-\rho)^2 + t(1-\rho)\right]\mathrm{d}W_e \tag{25}$$

$$b_6 = \left[\tfrac{1}{2}H_e\rho^2\lambda - \left(t - \Delta_p\rho\right)\left(2\psi - \tfrac{3}{2}\rho + 2\right)\right]\mathrm{d}W_e \tag{26}$$

In the above system of equations, rows 1 to 3 are horizontal force equilibrium equations, and rows 4 to 6 are moment equilibrium equations, for the top, middle and bottom blocks respectively.

We can reduce this system of equations and substitute in equations (10) and (12) to obtain the following condition which contains only the two unknowns $\mathrm{d}M_1$ and $\mathrm{d}M_2$:

$$\begin{aligned} \frac{1}{\gamma t^2 H_e} \cdot \frac{\mathrm{d}M_1 + \mathrm{d}M_2}{\mathrm{d}x} = {} & [2\psi\epsilon - 4\psi - 2] \\ & + \rho\left[4\psi\delta_p + 2\delta_p + 2\lambda\frac{H_e}{t}\right] \\ & + \rho^2\left[-\lambda\frac{H_e}{t}\right]. \end{aligned} \tag{27}$$

This expression represents the sum of the derivatives of longitudinal moments M_1 and M_2 for the top and bottom subpanels with respect to x (refer Figure 7b). However, since both of these subpanels have zero end moments at boundaries $x = 0$ and $x = L_e$, longitudinal moment equilibrium requires that the integral of equation (27) between these limits must also be zero, i.e.:

$$0 = \int_0^{L_e} \left(C_0 + C_1\rho + C_2\rho^2\right)\mathrm{d}x, \tag{28}$$

where polynomial coefficients C_0, C_1 and C_2 are the square bracket terms in equation (27). [Note that by contrast, the integral of $\mathrm{d}M_3$ along subpanel 3 is not zero as a consequence of the vertical edge moment reaction M_{3x} (Figure 7).] As shown in Figure 7d, shape parameter ρ varies along x such that

$$\rho = \begin{cases} x/L_d & \text{for } x \le L_d, \\ 1 & \text{for } L_d < x \le L_d + L_a, \end{cases} \tag{29}$$

where $L_d = (1-a)L_e$ and $L_a = aL_e$. Combining these expressions and evaluating integral (28) yields

$$0 = C_0 + C_1\left(\tfrac{1}{2} + \tfrac{1}{2}a\right) + C_2\left(\tfrac{1}{3} + \tfrac{2}{3}a\right). \tag{30}$$

Finally, we substitute coefficients C_0, C_1 and C_2 together with equations (11) and (16) into equation (30), and rearrange to get the rigid rocking relationship for the mechanism in terms of λ versus the central displacement δ_c:

$$\lambda_r(\delta) = \frac{t}{H_t} \cdot \frac{4\left[1 + \psi(2-\epsilon)\right] - \delta_c\left[2(1+a)(1+2\psi)\right]}{\tfrac{2}{3} + \tfrac{1}{3}a}. \tag{31}$$

The above formula follows the linear-descending form associated with rigid body rocking (dashed line in Figure 1) and is valid in the positive range of displacement. From this, the load capacity λ_{ro} is obtained by setting $\delta_c = 0$, and the instability displacement δ_{ru} (displacement capacity) is obtained by setting $\lambda_r = 0$.

The process demonstrated here on mechanism K2x can similarly be applied to any of the other two-way mechanisms shown in Figure 2 to produce the load and displacement capacities given in Table 1. The various input parameters throughout these equations are defined in Section 2. For details of these derivations the reader is referred to reference [26]. Over the full range of displacement, these idealised rocking relationships are given by

$$\lambda_r(\delta) = \begin{cases} \lambda_{ro}^{+}\left(1 - \delta/\delta_{ru}^{+}\right) & \text{for } \delta > 0, \\ 0 & \text{for } \delta = 0, \\ \lambda_{ro}^{-}\left(-1 - \delta/\delta_{ru}^{-}\right) & \text{for } \delta < 0. \end{cases} \tag{32}$$

Superscripts '+' or '–' are used simply to denote that the positive and negative direction capacities can be asymmetric due to precompression eccentricity effects.

A notable feature of these idealised rigid rocking relationships is that the resulting expressions for the load capacity (λ_{ro}) are identical to capacities that can be obtained using a virtual work approach in which internal work contributions are included only along horizontal and diagonal cracks (i.e. vertical cracks are excluded), and where these crack moment capacities are taken in the form $M/b = \sigma_v t^2/2$ (i.e. restoring moment lever arm taken as half the wall thickness) [8, 26]. In other words, the snapshot at $\Delta = 0$ obtained from such a virtual work analysis can be considered as a particular case of the rocking λ-δ relationships proposed in this paper.

Relationships for vertically spanning mechanisms V1 (free-standing wall) and V2 (simply-supported at top and bottom with crack at mid-height) are also given in Table 1 for reference. These are obtained as a particular case of the K1x and K2x solutions by setting $a = 1$. The resulting expressions are similar to those presented by [2] with the additional features of allowing for control over the precompression load eccentricity and restraint.

Table 1: Equations defining the idealised rigid block load-displacement relationship for the rocking component of response. Note that the instability displacement is taken at the reference location along the mechanism, indicated as Δ' in Figure 2.

Mech.	Overturning load λ_{ro}	Instability displacement δ_{ru}
K1x	$\lambda_{ro} = \frac{t}{H_t} \cdot \frac{\frac{3}{2} - \frac{1}{2}a + 2\psi(1 - a\epsilon)}{\frac{2}{3} + \frac{1}{3}a + \Phi\eta\psi(1 + a)}$	$\delta_{ru} = \frac{\frac{3}{2} - \frac{1}{2}a + 2\psi(1 - a\epsilon)}{\frac{2}{3} + \frac{1}{3}a + \psi(1 + a)}$
K1y	$\lambda_{ro} = \frac{t}{H_t} \cdot \frac{\frac{3}{2} + \frac{1}{2}r + 2\psi}{\alpha\left(\frac{2}{3} + \frac{1}{3}r + \Phi\eta\psi\right)}$	$\delta_{ru} = \frac{\frac{3}{2} + \frac{1}{2}r + 2\psi}{\frac{2}{3} + \frac{1}{3}r + \psi}$
K2x	$\lambda_{ro} = \frac{t}{H_t} \cdot \frac{4\left[1 + \psi(2 - \epsilon)\right]}{\frac{2}{3} + \frac{1}{3}a}$	$\delta_{ru} = \frac{2\left[1 + \psi(2 - \epsilon)\right]}{(1 + a)(1 + 2\psi)}$
K2y	$\lambda_{ro} = \frac{t}{H_t} \cdot \frac{4\left[1 + \psi(2 - \epsilon)\right]}{\alpha\left(\frac{2}{3} + \frac{1}{3}r\right)}$	$\delta_{ru} = \frac{2\left[1 + \psi(2 - \epsilon)\right]}{1 + 2\psi}$
V1	$\lambda_{ro} = \frac{t}{H_t} \cdot \frac{1 + 2\psi(1 - \epsilon)}{1 + 2\Phi\eta\psi}$	$\delta_{ru} = \frac{1 + 2\psi(1 - \epsilon)}{1 + 2\psi}$
V2	$\lambda_{ro} = \frac{t}{H_t} \cdot \{4\left[1 + \psi(2 - \epsilon)\right]\}$	$\delta_{ru} = \frac{1 + \psi(2 - \epsilon)}{1 + 2\psi}$

3.2.2. Rocking in Real Walls

The λ-δ relationships presented in the previous section were based on idealised rigid rocking behaviour. Real masonry walls differ from this in that they are deformable, possess geometric imperfections (non-flat contact surface across cracked sections), and have finite material compressive strength which can further lead to degradation of the crack interface under cyclic loading.

Due to finite material stiffness, response within the small displacement range prior to lift-off must be linear elastic, and thus the discontinuity across $\delta = 0$ inherent in the idealised rigid body model becomes avoided (refer Figure 1). Also, finite compressive strength means that force transfer between subpanels cannot be transmitted across a knife-edge interface, causing the actual internal lever arm resisting rocking to be less than the lever arm assumed in the rigid body case. These effects cause the actual capacity curve to become bounded by the prediction of idealised rigid body theory, which has been demonstrated experimentally for vertically spanning walls [3, 27]. (N.B. As will be shown later in Section 4.1, this is not entirely apparent in the experimental F-Δ behaviour observed in mortared two-way walls which can experience an enhancement in strength beyond the rigid body prediction; however this is due to other effects such as internal confinement and arching, and the logic of the statement still applies.)

In existing literature, alternate piecewise-linear F-Δ models have been proposed for non-rigid vertically spanning walls, including trilinear [2, 3, 18] or bilinear [19]. In this paper we will use the bilinear form (Figure 6a)—firstly for sake of simplicity and secondly because the transition displacements used to define a trilinear model are not clearly measurable from available experimental F-Δ behaviour data for two-way walls (e.g. [5]); therefore, the additional rigour of a trilinear model may not be justified.

Predicting the stiffness of the initial loading branch of a post-cracked wall is a challenging task, influenced by a variety of factors including the effective material stiffness and state of degradation at the cracked joints. For the purposes of comparing the model to experiment, the 'yield' displacement in the bilinear model (δ_y) will be approximated by averaging the transition displacements δ_1 and δ_2 as proposed by Doherty et al [2] for defining the trilinear model for vertically spanning walls (see Figure 1). These values are summarised in Table 2 for three different states of degradation. It will be shown later that the estimated F-Δ response resulting from this assumption is in fairly good agreement with experimental behaviour, even though this treatment is simplistic and does not provide a fully rational account of the influence of physical characteristics such as the wall's length, height and thickness on stiffness. More research is required in this area; however, for the purposes of computing dynamic response, time-history analysis studies undertaken in [2] have shown collapse to be relatively insensitive to the stiffness of the initial loading branch in the F-Δ model.

A reduced 'effective' wall thickness approach can be used to account for the finite bearing zone width across cracks. By adopting a rectangular stress block approach at the point of

Table 2: Empirically-derived limiting displacements δ_1 and δ_2 for the trilinear λ-δ relationship by Doherty et al [2]. Yield displacement δ_y is taken as the average of these two values.

State of degradation at the cracked joint	δ_1	δ_2	δ_y
New	0.06	0.28	0.17
Moderate	0.13	0.40	0.27
Severe	0.20	0.50	0.35

crushing, the thickness reduction factor (ratio of effective thickness to gross thickness) becomes

$$\phi_r = 1 - \frac{\sigma_v}{c\, f_{mc}}, \tag{33}$$

where σ_v is the average compressive stress along the section, f_{mc} is the compressive strength of the masonry (or mortar, whichever is weaker) and c is a reduction factor (typically taken as 0.85 in reinforced concrete design). Since both the rocking strength (λ_{ro}) and displacement (δ_{ru}) capacities are proportional to the thickness (t), factor ϕ_r reduces both in equal proportion, and hence the negative slope of the descending branch in Figure 6a remains unaltered; the branch only shifts inward.

3.3. Horizontal Bending Friction Component

Unlike vertically spanning walls whose F-Δ behaviour is nonlinear but elastic (i.e. unloading path follows loading path), response of two-way walls contains some component of inelastic hysteretic behaviour due to activation of frictional sources of resistance in the post-cracked state. This is evidenced by hysteresis loops observed in the F-Δ response of two-way walls tested both under quasistatic cyclic loading and by shaketable [5, 6]. In the interpretation of these test results, the observed inelastic behaviour was attributed to residual moment capacity in horizontal bending (i.e., vertical crack lines) by the mechanism of torsional friction across cracked bed joints.

As discussed in the previous section, the load capacity of the rocking component (λ_{ro}) is equivalent to applying the virtual work method at the limit $\delta = 0^+$ by including only resistances along horizontal and diagonal crack lines using the method described in [8]. By similarity, it is proposed that the resistance contribution of horizontal bending toward the overall F-Δ model can be incorporated in terms of an inelastic component, whose load capacity λ_{ho} can be predicted using a virtual work approach that only includes internal work contributions from moment along vertical cracks. Resulting expressions for the various mechanisms are provided in Table 3 (second column). Further detail of their derivation is provided in [26].

Throughout these equations, $\bar{Z}_h$ is the moment modulus per height of crack, which for regular overlapping masonry (Figure 3) is obtained as

$$\bar{Z}_h = \frac{\mu_m\, k_{bp}\, t_u^3}{h_u + t_j}, \tag{34}$$

where μ_m is the friction coefficient across the bed joint, k_{bp} is the plastic torsion coefficient for a rectangular section given by the following expression (0.383 for square overlap):

$$k_{bp} = \frac{1}{12}\Bigg[2r_o\sqrt{1+r_o^2} + \ln\left(r_o + \sqrt{1+r_o^2}\right) + r_o^3\,\ln\left(r_o^{-1} + \sqrt{1+r_o^{-2}}\right)\Bigg]. \tag{35}$$

In the above expression, r_o is the bed joint overlap ratio, which is dependent on the type of bonding pattern of the masonry. In the case of half-overlap masonry (Figure 3), it is equal to

$$r_o = \frac{s_b}{t_u} = \frac{l_u - t_j}{2t_u}. \tag{36}$$

Other input parameters in Table 3 include: moment fixity factor for supported vertical edges, R_{vs} (taken as 0 for pin-support or as 1 for fixed-support); and energy contribution factor for the central vertical crack, ζ_{hi}, to be taken as

$$\zeta_{hi} = \begin{cases} 0 & \text{if one vertical edge is supported } (n_{vs} = 1), \\ 1 & \text{if both vertical edges are supported } (n_{vs} = 2). \end{cases} \tag{37}$$

The parameter ζ_{hi} features in expressions for mechanisms K1y and K2y, and simply accounts for the fact that the central vertical crack only occurs when both vertical edges are supported.

The approach described makes the following assumptions (in addition to those listed in Section 3.1):

1. Moment capacities of vertical cracks are based on torsional friction along interlocking courses of bricks, with the instantaneous centre of rotation located at the centre of the bed joint.

2. All bed joints along the height of the vertical crack are assumed to fully contribute to the total crack moment. In mortared stretcher bond URM walls however, cracks tend to generally develop a mixture of stepped failure (interlocking cracks) and line failure (cracks passing through brick units), and only the stepped portions contribute toward residual capacity. A theoretical approach for estimating the relative likelihood of each type of failure is reported in [28], which could be used as the basis for a capacity reduction factor to account for these effects. Furthermore, it has been argued [29] that contributions of friction toward the out-of-plane collapse load should be treated in terms of bounds rather than unique solutions, and that the assumption of full frictional contribution provides only the upper limit of these bounds.

Table 3: Equations for load capacities of the inelastic (frictional) components.

Mech.	Load capacity of horizontal bending rotational friction, λ_{ho}	Load capacity of precompression load sliding friction, λ_{so}
K1x	$\lambda_{ho} = \frac{\bar{Z}_h G_n}{t_u L_e} \cdot \frac{R_{vs}(1+2\psi)}{\frac{2}{3}+\frac{1}{3}a+\Phi\eta\psi(1+a)}$	$\lambda_{so} = (1-\Phi)\frac{\mu_o\psi(1+a)}{\frac{2}{3}+\frac{1}{3}a}$
K1y	$\lambda_{ho} = \frac{\bar{Z}_h G_n}{t_u L_e} \cdot \frac{R_{vs}(1+2\psi)+\zeta_{hi}r(r+2\psi)}{\alpha\left(\frac{2}{3}+\frac{1}{3}r+\Phi\eta\psi\right)}$	$\lambda_{so} = (1-\Phi)\frac{\mu_o\psi}{\frac{2}{3}+\frac{1}{3}r}$
K2x	$\lambda_{ho} = \frac{\bar{Z}_h G_n}{t_u L_e} \cdot \frac{2R_{vs}(1+2\psi)}{\frac{2}{3}+\frac{1}{3}a}$	$\lambda_{so} = 0$
K2y	$\lambda_{ho} = \frac{\bar{Z}_h G_n}{t_u L_e} \cdot \frac{2(R_{vs}+\zeta_{hi}r)(1+2\psi)}{\alpha\left(\frac{2}{3}+\frac{1}{3}r\right)}$	$\lambda_{so} = 0$
V1	$\lambda_{ho} = 0$	$\lambda_{so} = (1-\Phi)(2\mu_o\psi)$
V2	$\lambda_{ho} = 0$	$\lambda_{so} = 0$

3. Frictional slip along vertical cracks is assumed to be purely torsional (a requirement for general assumption No. 2 in Section 3.1). This approximation however ignores potential translational slip that could develop along vertical cracks, particularly in zones of high out-of-plane shear force. For example, in the test study reported in [5], sliding of the main panel away from flanking return walls was observed in a small number of cases, and this effect was most evident in instances where a large proportion of brick units ruptured by line failure. Although kinematic mechanisms with pure translational slip at the vertical edges are not considered in this paper, their resistance may be computed independently to assess whether they are likely to govern (e.g. using method described in [19]).

4. Equations (34) and (36) assume that bed joints retain full overlap over a section with dimensions $s_b \times t_u$. However, from geometry it follows that to maintain a constant L under an out-of-plane displacement, the wall must undergo some longitudinal slip between its subpanels (along x direction, refer Figure 7), thus reducing the area of the contact interfaces. For walls with large L/t aspect ratios, this effect is expected to be negligible over the displacement range of interest. However, in walls where loss of overlap might be expected to be significant (small L/t), k_{bp} could be calculated using a reduced overlap section to allow for this effect.

5. The derived frictional capacities are based on the assumption that the vertical stress at the level of the crack is equivalent to the undisturbed stress (precompression plus weight of panel above). However, it is conceivable that in mortared walls, the continued cyclic rotation of interlocking cracks can degrade the bed joint interfaces, which can relieve the axial stress acting across them. Additional experimental testing is required to investigate the importance of this effect.

To account for the above assumptions and approximations in practical design or assessment, it may be prudent to reduce the nominal λ_{ho} capacities in Table 3. Derivation of such reduction factors however is beyond the scope of this paper.

In the overall λ-δ model we shall represent the contribution from horizontal bending [$\lambda_h(\delta)$ in equation (9)] using elastoplastic hysteresis (Figure 6b). Due to the lack of a more sophisticated model to predict the initial loading stiffness of a cracked masonry wall (as discussed in Section 3.2.2), it is suggested that the elastoplastic yield displacement can be estimated using the same approach as for the rocking component; that is, according to the δ_y limits in Table 2.

3.4. Precompression Load Frictional Sliding Component

As discussed in Section 2.2, in mechanism K1 it is possible for a wall to benefit from an additional source of resistance due to frictional sliding between the wall and precompression load. In order for this resistance to be activated, a frictional connection must exist at the interface, and the precompression load must be laterally restrained (Figure 4a). Furthermore, the restraining friction must be sufficiently low to prevent the wall from transitioning to mechanism K2.

The load capacity contribution from precompression sliding is given as λ_{so} in Table 3, which can be determined either by the statics method used previously for rocking (Section 3.2.1) or from a virtual work approach as shown elsewhere [26]. If this resistance can be maintained under increasing wall displacement then this component of response can be incorporated into the overall capacity curve using an elastoplastic rule (As shown in Figure 6b but using λ_{so} as the load capacity).

3.5. Complete Model

Using equation (9) the complete hysteresis model is obtained by superimposing the load contributions of the elastic rocking component (Figure 6a), frictional component from horizontal bending (Figure 6b), and if present, frictional sliding between the wall and precompression load. The resulting hysteresis shape and capacity envelope of the combined model are shown by Figure 9. For illustrative purposes, points (4)-(12) on Figure 9 demonstrate a hysteresis loop formed during a full cycle at amplitude $\pm\delta_{\text{amp}}$.

4. Comparison with Experimental Data

To verify the accuracy of the proposed model, the predicted F-Δ response was compared to behaviour of two-way walls tested experimentally. Two separate data sets were considered: quasistatic cyclic tests on eight full-scale, clay brick, mortared walls [5], and monotonic tests on three half-scale, clay brick, dry-stack (unmortared) walls [30]. In both sets of tests, loading was applied using airbags, and all walls underwent the relevant type K mechanism (Figure 2).

For each wall and its associated mechanism, capacities λ_{ro}, δ_{ru} and λ_{ho} were calculated using the formulae in Tables 1 and 3. In walls that had precompression, frictional slip at the top edge was not observed in the tests; thus, type K1 mechanisms with the λ_s component were not considered. The predicted capacities are unfactored, in that they do not incorporate for any of the additional capacity reduction effects discussed in Sections 3.2 and 3.3.

Summaries of the analyses are presented in Tables 4 and 5. Graphical comparison between predicted and experimental behaviour is provided in Figures 10 and 11. Throughout these figures, the predicted rigid body rocking component (λ_r) is indicated by a coloured (red or blue) solid line. Response inclusive of the additional inelastic contribution from horizontal bending ($\lambda_r \pm \lambda_{ho}$) is shown by dashed lines for the forward and reverse loading directions. The enclosed shaded area represents the area of a hysteresis loop under reversed cyclic loading. Initial loading branches based on Doherty's empirical δ_y limits are also shown for the three different damages states (Table 2).

Key aspects of the undertaken analyses are as follows:

- For each solid wall (i.e. without openings), the length and height spans of the mechanisms (L_t and H_t) were taken as the full dimension of the wall. This was consistent with the experimentally observed crack patterns.
- Since the equations in Tables 1 and 3 assume the wall to be solid, two alternate approaches were used to estimate the capacities of walls with openings: The first approach ignored the openings and treated the wall as entirely solid. The second approach treated the wall as if it had a free vertical edge at boundary between the panel and the opening. In the latter treatment, only the longer side of the wall was analysed since this results in the governing (lower) capacity.

4.1. Mortar-Bonded Walls (Cyclic Tests)

This data set comprised eight full-scale, mortared brick masonry walls as reported in [5]. Of the eight walls (S1-S8), walls S1, S3, S4, and S7 were subjected to vertical precompression (ψ between 1.06–2.11) applied using a loading pin at the mid-thickness of the wall (therefore $\epsilon = 0.5$). Walls S1-S2 were solid and S3-S8 each had a single window opening. The walls were supported along all four edges, with the exception of wall S6 which was free at the top edge. The vertical edges of each wall were restrained against rotation by means of a clamping arrangement along the vertical edge of short return walls; therefore, the calculations assume full rotational fixity ($R_{vs} = 1$).

A notable aspect of the experimental F-Δ behaviour was the positive tangent stiffness (slope) of loading coupled with strength and stiffness degradation with increasing cyclic displacement (Figure 10). This is thought to have been caused by internal confinement (arching) effects; specifically, a combination of horizontal confinement from in-plane restraint provided by vertical edge supports, and vertical confinement of the bottom and top mechanism subpanels by the left and right subpanels close to the supported vertical edges. Because of this effect, the experimental F-Δ response did not exhibit a distinct value of residual post-cracked strength. It therefore becomes more convenient to compare the observed and predicted response graphically, as shown in Figure 10. Details of the analyses are summarised in Table 4.

The following observations can be made from these comparisons:

1. The proposed model provides a conservative lower-bound representation of each wall's F-Δ response envelope over the full range of displacement to which the walls were subjected. This conservatism is thought to be due to the activation of internal arching within the walls as discussed above.

2. The model appears to underpredict the inelastic (frictional) capacity of the walls, as can be seen by comparing the experimental hysteresis loops to the predicted forward and reverse path branches (shaded areas enclosed by dashed lines in Figure 10). This is also likely due to the internal arching effects in the tested walls causing additional compressive stress and therefore enhancement of frictional resistance. Additionally, real wall behaviour is also likely to include some component of torsional friction acting on

Table 4: Details of analyses performed on quasistatic test walls S1–S8 (from reference [5]).

Wall	Treatment*	Input parameters					Intermediate variables							Mech.	Calculated capacities		
		L_t [mm]	H_t [mm]	σ_{vo} [MPa]	ϵ	R_{vs}	L_e [mm]	H_e [mm]	α	a	r	ψ	ζ_{hi}		δ_{ru}	λ_{ro}	λ_{ho}
S1, S3	solid	4080	2494	0.1	0.5	1	2040	1247	1.17	0.15	-	2.11	-	K2x	1.39	1.03	0.29
S3	longer side	2220	2494	0.1	0.5	1	2220	1247	1.28	0.22	-	2.11	-	K2x	1.31	0.99	0.25
S4	solid	4080	2494	0.05	0.5	1	2040	1247	1.17	0.15	-	1.06	-	K2x	1.45	0.64	0.17
S4	longer side	2220	2494	0.05	0.5	1	2220	1247	1.28	0.22	-	1.06	-	K2x	1.37	0.62	0.15
S2, S5	solid	4080	2494	0	-	1	2040	1247	1.17	0.15	-	0	-	K2x	1.74	0.25	0.05
S5	longer side	2220	2494	0	-	1	2220	1247	1.28	0.22	-	0	-	K2x	1.64	0.24	0.05
S6	solid	4080	2494	0	-	1	2040	2494	0.59	-	0.41	0	1	K1y	2.12	0.16	0.05
S6	longer side	2220	2494	0	-	1	2220	2494	0.64	-	0.36	0	0	K1y	2.14	0.15	0.04
S7	solid	2520	2494	0.1	0.5	1	1260	1247	0.72	-	0.28	2.11	1	K2y	1.60	1.34	0.77
S7	longer side	660	2494	0.1	0.5	1	660	1247	0.38	-	0.62	2.11	0	K2y	1.60	2.22	1.91
S8	solid	2520	2494	0	-	1	1260	1247	0.72	-	0.28	0	1	K2y	2.00	0.32	0.15
S8	longer side	660	2494	0	-	1	660	1247	0.38	-	0.62	0	0	K2y	2.00	0.53	0.37

Input constants
Unit geometry: l_u = 230 mm, t_u = 110 mm, h_u = 76 mm, t_j = 10 mm
Material properties: γ = 19 kN/m^3, μ_m = 1.04

Dependent constants
Natural diagonal slope: G_n = 0.717
Overlap ratio: r_o = 1; Plastic torsion coefficient: k_{bp} = 0.383
Horizontal bending moment modulus: $\bar{Z}_h$ = 6140 mm^3/mm

*Refers to the treatment used for walls with openings: In the 'solid' treatment any openings present were entirely ignored. In the 'longer side' treatment, the wall was treated as if it had a free vertical edge at the boundary of the opening.

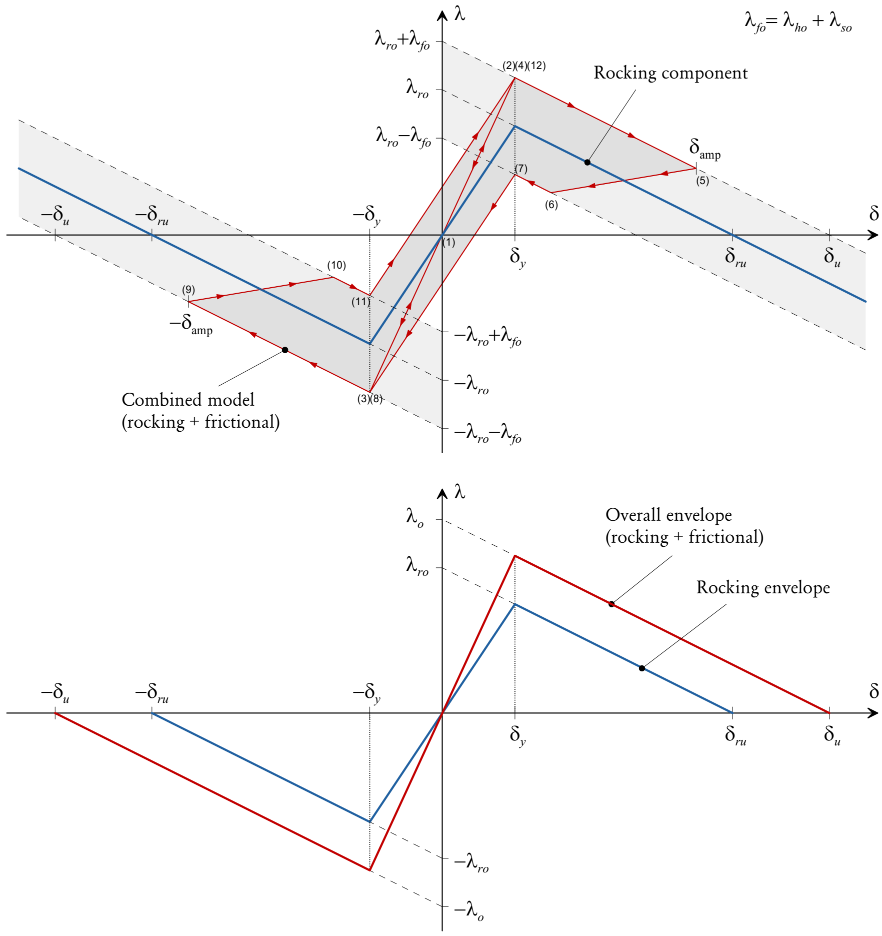

Figure 9: Complete load-displacement model obtained by superposition of the rocking and frictional components.

bed joints along diagonal crack lines, particularly at small rotations before the cracks fully open. This source of resistance is not considered in the model.

3. In walls with openings, the difference in predictions using the two alternative approaches (solid wall analysis versus longer side analysis) is relatively minor in walls S3, S4, S5 and S6, but more pronounced in walls S7 and S8. The sensitivity of the predicted load capacities relates to the value of the effective length (L_e) used as input in the respective treatments (refer to Table 4).

   It is suggested that a more refined approach for analysing walls with openings would be to calculate λ_{ro} and λ_{ho} using a virtual work treatment which considers the presence of the openings (e.g. as described in [8]); whilst still using the relationships in Table 1 to estimate the instability displacement δ_{ru}.

4. By visual comparison, the initial loading branches obtained using the empirical δ_y limits (Table 2) appear to provide an acceptable representation of the measured curves at continually increasing levels of stiffness degradation.

4.2. Dry-Stack Masonry Walls (Monotonic Tests)

This set of data comprised three half-scale, dry-stack brick walls as reported in [30]. The clay units used to build the walls were obtained by cutting solid paving units, and this process introduced some irregularities in the shape of the resulting units; thus, the walls could be considered representative of very poor quality masonry construction. Each wall (F1-F3) was supported at four edges and had short return walls. Unlike in the cyclic tests discussed in Section 4.1, these return walls were not clamped and therefore the vertical edges were only partially restrained against rotation. For comparison purposes however, full rotational fixity is assumed at the vertical edges ($R_{vs} = 1$). Each wall was tested at three varying levels of precompression (ψ ranging between 1.75–4.75) applied using a loading pin at mid-thickness ($\epsilon = 0.5$). The walls were loaded monotonically, and intermittently unloaded to study their hysteretic behaviour. None of these walls were tested to failure; however, the largest imposed displacement δ in each test ranged between 0.5 and 1.

A summary of the analyses is presented in Table 5, and the predictions are compared to experiment graphically in Figure 11. It can be seen that the experimental response of the walls under unloading is inelastic, indicating that frictional resistance was activated. These curves exhibit a clear peak load followed

Table 5: Details of analyses performed on half-scale dry-stack masonry test walls F8–F10 (from reference [30]). The walls have translational restraint along all four edges and assumed moment fixity along the vertical edges (refer to discussion in text).

Wall	Treatment*	Input parameters					Intermediate variables							Mech.	Calculated capacities		
		L_t [mm]	H_t [mm]	σ_{vo} [MPa]	ϵ	R_{vs}	L_e [mm]	H_e [mm]	α	a	r	ψ	ζ_{hi}		δ_{ru}	λ_{ro}†	λ_{ho}†
F8	solid	2180	960	0.036	0.5	1	1090	480	1.18	0.16	-	1.86	-	K2x	1.39	0.92	0.15
				0.046								2.37			1.37	1.11	0.18
				0.066								3.40			1.35	1.48	0.25
F9	solid	1720	960	0.034	0.5	1	860	480	0.93	-	0.07	1.75	1	K2y	1.61	1.14	0.25
				0.055								2.84			1.57	1.64	0.37
				0.080								4.13			1.55	2.25	0.51
F10	solid	1950	750	0.028	0.5	1	975	375	1.36	0.26	-	1.85	-	K2x	1.27	1.08	0.15
				0.050								3.30			1.24	1.70	0.25
				0.072								4.75			1.23	2.33	0.34

Input constants
Unit geometry: l_u = 115 mm, t_u = 55 mm, h_u = 30 mm, t_j = 0 mm
Material properties: γ = 20.2 kN/m^3, μ_m = 0.761

Dependent constants
Natural diagonal slope: G_n = 0.522
Overlap ratio: r_o = 1.05; Plastic torsion coefficient: k_{bp} = 0.409
Horizontal bending moment modulus: $\bar{Z}_h$ = 1727 mm^3/mm

*Refer to note in Table 4.
†These load capacities were obtained by reducing the nominal load capacities (calculated using equations in Tables 1 and 3), to account for the fact that the airbag arrangement in the tests did not cover the entire wall face and was concentrated nearer to the centre. The applied reduction factor was calculated as the ratio of the average virtual displacement along the loaded area in the respective loading scenarios, and was computed as 0.761, 0.879 and 0.736 for walls F8-F10 respectively.

by a softening branch, which is consistent with the general form of the proposed F-Δ model. It is evident that any internal arching in these walls was minimal, contrary to the response of the mortared walls (refer Section 4.1).

Interestingly, the idealised rigid block load capacity λ_{ro} overestimates the measured strength in each of these walls, which is thought to be due to the poor quality of the brick units, as stated previously. As seen from Figure 1, the ratio of the peak load capacity in Doherty's trilinear model to the idealised rigid block capacity (λ_{ro}) is equivalent to $1 - \delta_2$. According to the empirically-derived limits (Table 2), a load capacity ratio of 0.5 would be expected for severely degraded masonry, which is comparable to the trends evident in these walls. For comparison purposes, the upper bound dashed lines ($\lambda_r + \lambda_h$) in Figure 11 show the expected response by including full participation of the horizontal bending capacity component; however as stated earlier, it is likely that these vertical edges behaved more as pinned rather than fixed. Thus the overall behaviour is expected to lie closer to pure rocking response (λ_r).

Although the test walls were not pushed to collapse, the graphical comparisons in Figure 11 suggest that if the softening branches of the experimental F-Δ curves were extrapolated, then in most cases, the predicted displacement capacity (δ_{ru}) would provide a conservative estimate of the walls' displacement capacities.

5. Concluding Remarks

This paper has described a nonlinear inelastic load-displacement model for representing the behaviour of two-way spanning walls subjected to out-of-plane loading. The model ignores any initial bond strength and assumes that response consists of several independently acting resistance sources whose load contributions can be superimposed at any value of the wall's displacement. These include the rocking component, modelled as bilinear-softening; and frictional components due to horizontal bending and precompression load sliding, both modelled as elastoplastic.

A generalised method for predicting the load and displacement capacities of the rocking component of response has been described. The approach treats the wall as a series of vertically spanning strips held together by kinematic compatibility dictated by the shape of the collapse mechanism. The method has been applied to the type K family of mechanisms (refer to Figure 2) which is commonly associated with mortar-bonded walls; it is possible, however, to apply the same technique to other types of mechanisms. Expressions for the load capacities of the frictional components were obtained using the virtual work approach. By contrast, a fully rational and mechanics-based approach for calculating the initial loading branches based on a wall's post-cracked stiffness is still lacking and warrants future research.

Comparison of the proposed model with experimental F-Δ behaviour has been shown to be favourable—the model provides a reasonable albeit conservative representation of the capacity of mortared URM walls, and its general characteristics are also consistent with tests on dry-stack masonry walls. Furthermore, the components included in the model are consistent with the limit analysis principles applied to vertically spanning walls in other works (e.g. [2]) whilst allowing for benefits of two-way response.

Potential applications of the developed model include incorporation into a nonlinear time-history analysis for the stepwise computation of response under dynamic loading; or implementation as part of a displacement-based seismic design/assessment framework, for example using the capacity spectrum method in combination with the substitute structure concept. A conceptual demonstration of the latter is provided in [26].

Acknowledgements

This research was conducted with the financial support of the Australian Research Council (Grant No. DP0450933) and The University of Adelaide.

References

[1] R. D. Ewing, J. C. Kariotis, Methodology for mitigation of seismic hazards in existing unreinforced masonry buildings: Wall testing, out-of-plane, Tech. Rep. ABK-TR-04, ABK, A Joint Venture, El Segundo, California (Aug 1981).

[2] K. Doherty, M. C. Griffith, N. Lam, J. Wilson, Displacement-based seismic analysis for out-of-plane bending of unreinforced masonry walls, Earthquake Engineering and Structural Dynamics 31 (4) (2002) 833–850.

[3] H. Derakhshan, M. C. Griffith, J. M. Ingham, Out-of-plane behavior of one-way spanning unreinforced masonry walls, Journal of Engineering Mechanics 139 (4) (2013) 409–417.

[4] O. Penner, K. J. Elwood, Out-of-plane dynamic stability of unreinforced masonry walls in one-way bending: shake table testing, Earthquake Spectra 32 (3) (2016) 1675–1697.

[5] M. C. Griffith, J. Vaculik, N. T. K. Lam, J. Wilson, E. Lumantarna, Cyclic testing of unreinforced masonry walls in two-way bending, Earthquake Engineering and Structural Dynamics 36 (6) (2007) 801–821.

[6] J. Vaculik, M. C. Griffith, Shaketable tests on masonry walls in two-way bending, in: Australian Earthquake Engineering Society Conference, Wollongong, NSW, Australia, 2007.

[7] D. D'Ayala, E. Speranza, Definition of collapse mechanisms and seismic vulnerability of historic masonry buildings, Earthquake Spectra 19 (3) (2003) 479–509.

[8] J. Vaculik, M. C. Griffith, G. Magenes, Dry stone masonry walls in bending—Part II: Analysis, International Journal of Architectural Heritage 8 (1) (2014) 29–48.

[9] M. J. N. Priestley, G. M. Calvi, M. J. Kowalsky, Displacement-Based Seismic Design of Structures, IUSS Press, Pavia, Italy, 2007.

[10] M. J. N. Priestley, G. M. Calvi, M. J. Kowalsky, Direct displacement-based seismic design of structures, in: 2007 NZSEE Conference, 2007.

[11] S. A. Freeman, Review of the development of the capacity spectrum method, ISET Journal of Earthquake Technology 41 (1) (2004) 1–13.

[12] G. W. Housner, The behaviour of inverted pendulum structures during earthquakes, Bulletin of the Seismological Society of America 53 (2) (1963) 403–417.

[13] M. J. N. Priestley, R. J. Evison, A. J. Carr, Seismic response of structures free to rock on their foundations, Bulletin of the New Zealand National Society for Earthquake Engineering 11 (3) (1978) 141–150.

[14] N. Makris, D. Konstantinidis, The rocking spectrum and the limitations of practical design methodologies, Earthquake Engineering and Structural Dynamics 32 (2) (2003) 265–289.

[15] New Zealand Society for Earthquake Engineering, Assessment and Improvement of the Structural Performance of Buildings in Earthquakes, incl. corrigendum no. 3 Edition, 2014.

[16] L. Sorrentino, S. Kunnath, G. Monti, G. Scalora, Seismically induced one-sided rocking response of unreinforced masonry façades, Engineering Structures 30 (8) (2008) 2140–2153.
[17] M. C. Griffith, G. Magenes, G. Melis, L. Picchi, Evaluation of out-of-plane stability of unreinforced masonry walls subjected to seismic excitation, Journal of Earthquake Engineering 7 (S1) (2003) 141–169.
[18] N. T. K. Lam, M. Griffith, J. Wilson, K. Doherty, Time-history analysis of URM walls in out-of-plane flexure, Engineering Structures 25 (6) (2003) 743–754.
[19] S. Lagomarsino, Seismic assessment of rocking masonry structures, Bulletin of Earthquake Engineering 13 (1) (2015) 97–128.
[20] L. R. Baker, Structural action of brickwork panels subjected to wind loads, Journal of the Australian Ceramic Society 9 (1) (1973) 8–13.
[21] H. W. H. West, H. R. Hodgkinson, B. A. Haseltine, The resistance of brickwork to lateral loading, Part 1: Experimental methods and results of tests on small specimens and full sized walls, The Structural Engineer 55 (10) (1977) 411–421.
[22] S. J. Lawrence, Behaviour of brick masonry walls under lateral loading, PhD thesis, The University of New South Wales (1983).
[23] D. P. Abrams, R. Angel, J. Uzarski, Out-of-plane strength of unreinforced masonry infill panels, Earthquake Spectra 12 (4) (1996) 825–844.
[24] S. Lawrence, R. Marshall, Virtual work design method for masonry panels under lateral load, in: 12th International Brick and Block Masonry Conference, Vol. 2, Madrid, Spain, 2000, pp. 1063–1072.
[25] Comité Européen de Normalisation, Eurocode 6, Design of Masonry Structures—Part 1-1: General rules for reinforced and unreinforced masonry structures, EN 1996-1-1:2005 (E) Edition, CEN, Brussels, Belgium, 2005.
[26] J. Vaculik, Unreinforced masonry walls subjected to out-of-plane seismic actions, PhD thesis, The University of Adelaide (2012).
[27] M. C. Griffith, N. T. K. Lam, J. L. Wilson, K. Doherty, Experimental investigation of unreinforced brick masonry walls in flexure, Journal of Structural Engineering 130 (3) (2004) 423–432.
[28] J. Vaculik, M. C. Griffith, Probabilistic analysis of unreinforced brick masonry walls subjected to horizontal bending, Journal of Engineering Mechanics (In Press).
[29] C. Casapulla, Lower and upper bounds in closed form for out-of-plane strength of masonry structures with frictional resistances, in: 6th International Conference on Structural Analysis of Historical Constructions, Bath, UK, 2008, pp. 1191–1206.
[30] J. Vaculik, M. C. Griffith, B. Hogarth, J. Todd, Out-of-plane flexural response tests using dry-stack masonry, in: Australian Earthquake Engineering Society Conference, Mt Gambier, South Australia, 2004.

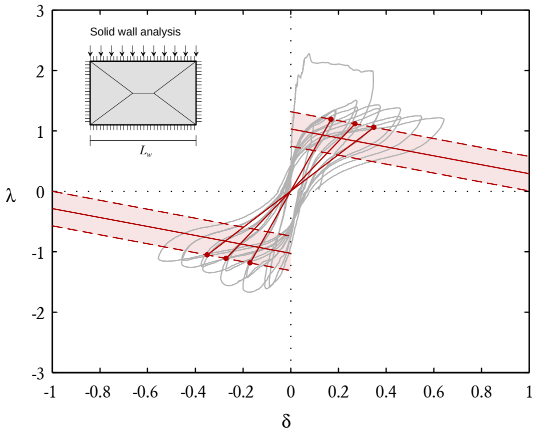

(a) Wall S1

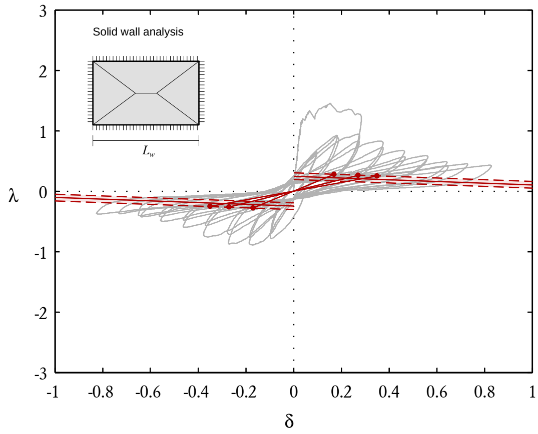

(b) Wall S2

Figure 10: Comparison of theoretical and experimental behaviour for mortared test walls S1–S8 from reference [5].

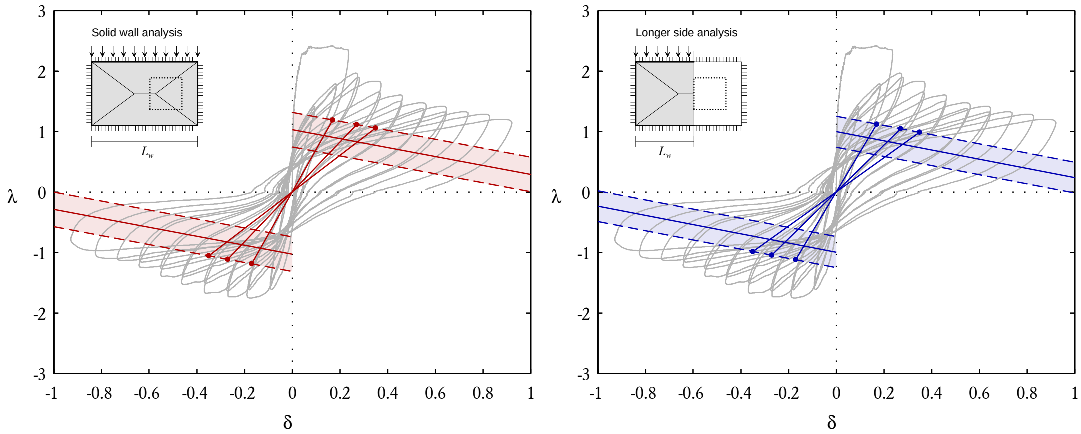

(c) Wall S3

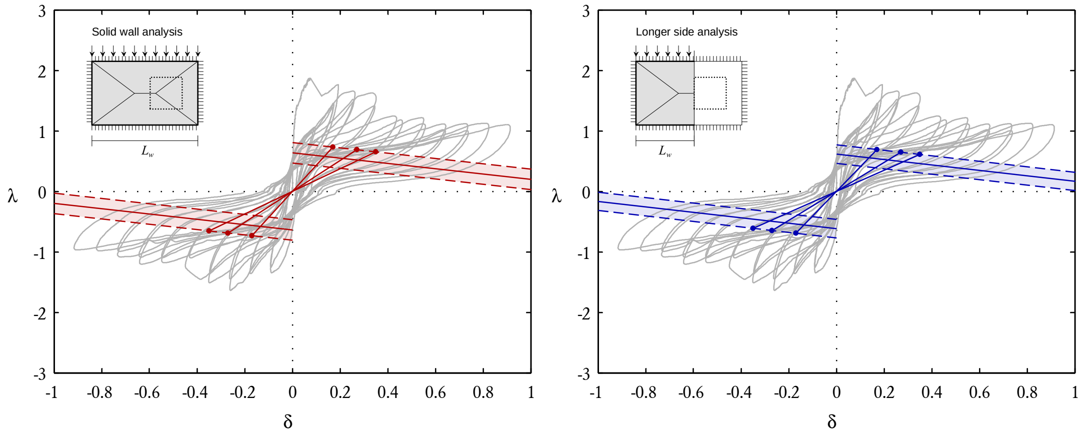

(d) Wall S4

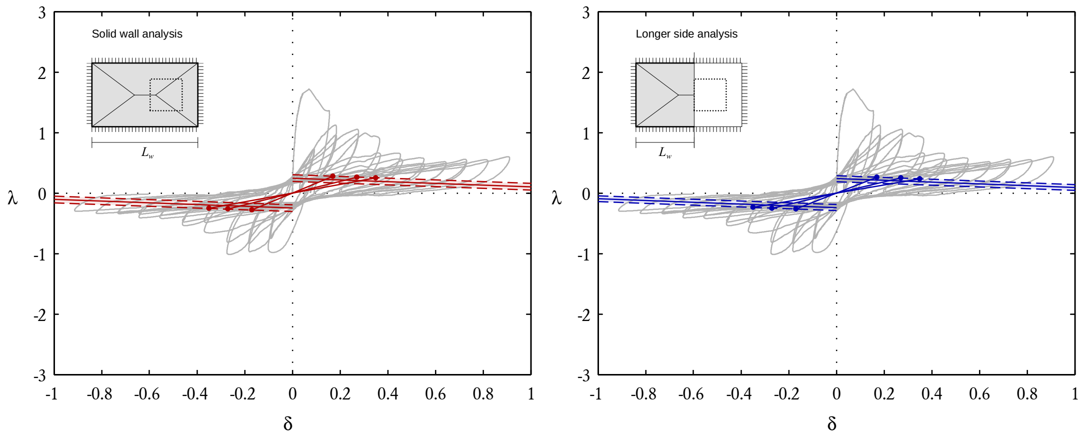

(e) Wall S5

Figure 10: (continued)

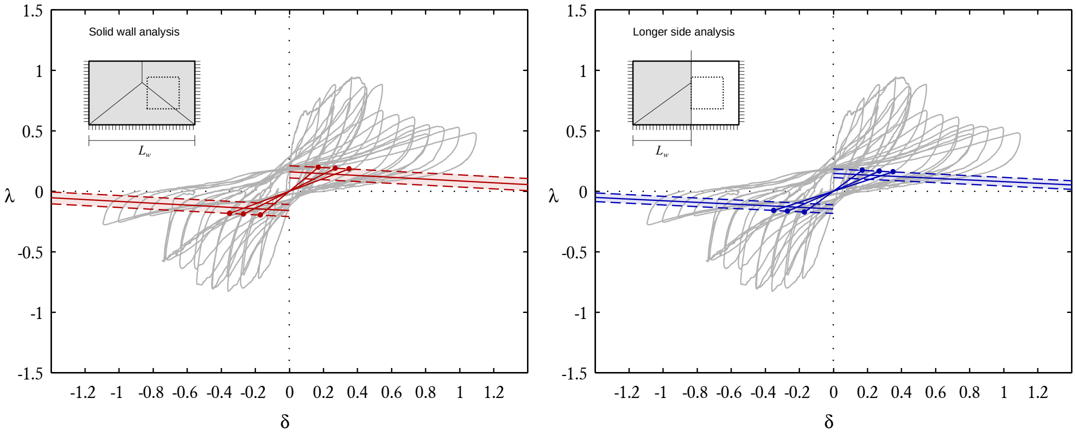

(f) Wall S6

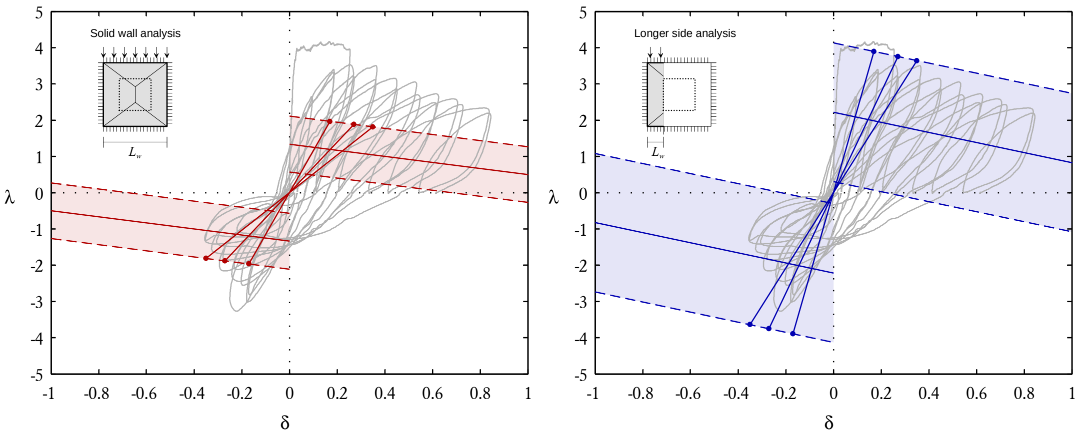

(g) Wall S7

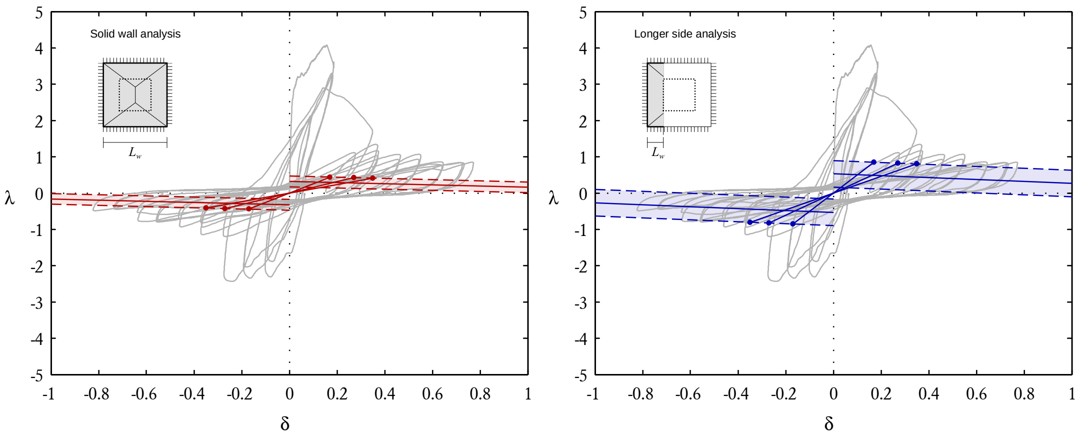

(h) Wall S8

Figure 10: (continued)

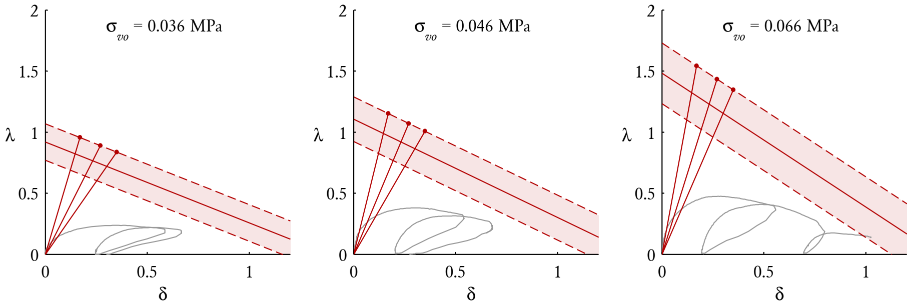

(a) Wall F8

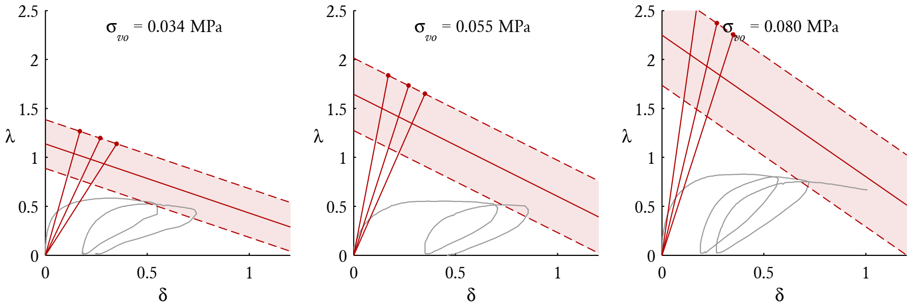

(b) Wall F9

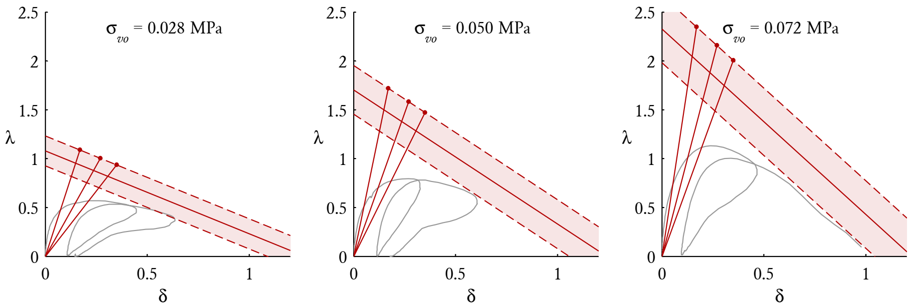

(c) Wall F10

Figure 11: Comparison of theoretical behaviour and experimental response for reduced-scale dry-stack masonry walls as reported in reference [30].